

OF-VO: Reliable Navigation among Pedestrians Using Commodity Sensors

Jing Liang, Yi-Ling Qiao, Tianrui Guan and Dinesh Manocha

Abstract—We present a novel algorithm for safe navigation of a mobile robot in uncertain environment among pedestrians. Our approach uses commodity visual sensors, including mono-camera and a 2D lidar, for explicitly predicting the velocities and positions of surrounding obstacles through optical flow estimation, object detection and sensor fusion. Given these probabilistic partial observations of the environment, we present a modified velocity-obstacle (VO) algorithm to compute velocities to navigate robot as it approaches to target. A key aspect of our work is coupling the perception (OF: optical flow) and planning (VO) components for reliable navigation. Overall, our OF-VO algorithm is a hybrid combination of learning-based and model-based methods and offers better performance than prior algorithms in terms of navigation time and success rate of collision avoidance. We highlight the realtime performance of OF-VO in simulated and real-world dynamic scenes on a Turtlebot robot navigating among pedestrians with commodity sensors. A demo video is available at <https://www.youtube.com/watch?v=5sYhZrGwsxM>

I. INTRODUCTION

Mobile robots are currently deployed in a wide range of scenarios including warehouses, airports, malls, and offices[1]. In these indoor and outdoor spaces, robots are used to perform routine tasks such as delivering goods and guiding customers. The ability to perform reliable navigation and avoid collisions with pedestrians and other obstacles is important for those tasks.

There are extensive works on robot navigation and collision-avoidance in dynamic scenes [2], [3]. These include model-based techniques based on velocity obstacles[4], dynamic constraints [2], etc. However, these methods assume the accurate detection of obstacles in the environment [4], [2]. Other techniques have been proposed for dynamic scenes [3], [5], but their performances vary in different environments and none of them are robust enough for all general scenarios [6]. Furthermore, some methods [7] rely on very expensive sensors like RTK-GPS or 3D Lidars.

Recently, a number of learning-based approaches have been proposed to perform robot navigation and collision avoidance [8], [9], [10]. These algorithms can handle sensor noise in many scenarios. However, it is challenging to predict the performance in new or unknown scenes with those learning-based models, because they could be biased towards the training data. Therefore, explainability and interpretability are essential aspects of a good navigation algorithm. Some model-based navigation algorithms [11] can provide these capabilities, although they may not work in terms of handling complex scenarios or sensor data.

Main Results: We present a novel hybrid scheme for safe navigation of a mobile robot among pedestrians and other



Fig. 1. Navigation among pedestrian in an indoor scene: We highlight the scene captured using a commodity camera mounted on the robot. The image on the left shows the segmentation of pedestrians with colored optical flow computed by our algorithm. Blue and red arrows correspond to pedestrian velocities. The curved black arrow represents the robot trajectory computed using our probabilistic collision avoidance algorithm. The image on the right highlights the environment, where the robot navigates amongst the pedestrians.

obstacles. Our approach take advantage of learning-based methods to handle sensor data and a model-based formulation to compute safe velocities for collision avoidance. Instead of developing an end-to-end approach, we use separate components for perception and planning. The novel components of our approach include:

- We combine a segmentation network and an optical flow network to detect static and dynamic obstacles with a pre-trained model. Our networks are fast enough to be deployed for real-time navigation.
- We present a modified velocity obstacle algorithm to perform local navigation and collision avoidance based on partial observations.
- We present bounds on probabilistic collision avoidance of our overall navigation algorithm (OF-VO) that take into account the sensor errors. Based on these bounds, we choose the time intervals to provide a given confidence in terms of collision avoidance.

We have tested our algorithm on a Turtlebot robot with cheap commodity sensors including an Orbecc Astra RGB camera, (around 100\$), and a 2-D Hokuyo Lidar, (around 1000\$). We have evaluated OF-VO in simulated and real-world environments with multiple pedestrians, including high-density environments with more than 10 pedestrians in a $5 \times 5m^2$ scenario. We have also compared our method with prior model-based methods like DWA [2] and deep-reinforcement learning algorithms like [12], and achieve at most $2 - 5X$ improvement in success rate (and reliability) and around 40% reduction in the navigation time in complex scenarios.

II. BACKGROUND AND RELATED WORK

In this section, we briefly survey related work on local navigation and collision avoidance. We also give an overview

of prior work in computer vision on object segmentation and motion detection.

A. Collision Avoidance

Many researchers have proposed learning-based algorithms for robot collision avoidance in real-world scenarios. [13] uses POMDPs to navigate robots in uncertain scenarios. [9] and [10] use deep learning to train end-to-end networks in indoor scenarios. These methods have shown good performance in terms of avoiding static obstacles. However, these methods can't handle complex dynamic scenes well, especially when the pedestrians are moving at different speeds.

With the development of reinforcement learning methods, policies can be trained for different sensors mounted on a robot. Cameras are widely used as inputs to reinforcement learning algorithms. For RGB cameras, [14] uses deep double-Q and [15] uses the A3C algorithm to train policies in cluttered scenarios. [12] uses 2D lidar along with the PPO algorithm [16] to navigate multiple robots in scenarios with static and dynamic obstacles. Some deep reinforcement learning-based navigation algorithms use a combination of cameras and 2d lidar [8]. However, these methods can result in oscillation or freezing issues during navigation and it is hard to provide any guarantees on their performance in general scenarios.

Many model-based algorithms [4], [2], [17] for collision avoidance have been proposed for motion planning in dynamic scenarios. However, these methods assume accurate detection and localization of obstacles. Moreover, in real world scenarios there are perception errors due to sensor noise and environment complexity. To address these inaccuracies, [18] propose a time-to-collision algorithm for reciprocal collision avoidance, but it may not work well in dynamic environments. [19] uses a receding horizon control algorithm with different constraints to navigate robots in uncertain environments. However, this approach can be time consuming as the algorithm needs to compute several consecutive actions in one step. [11], [20] use velocity obstacles for collision avoidance. However, these methods assume complete observations of nearby obstacles and environments.

B. Motion Estimation

Estimating the positions and velocities of moving objects plays an important role in navigation algorithm. Previous works [8] estimate velocities through trajectory tracking and prediction. However, tracking algorithms may not perform consistently well in dense scenes. They may lose tracking targets [21] and may result in inaccurate position and velocity estimations. Instead, we break down the motion perception into two stages, optical flow estimation and object detection.

Optical flow (OF) is the displacement of the pixel position between two consecutive images. Sparse OF only computes the flow on some landmark points, which takes less time. For real-time performance, methods [22] use sparse OF to avoid collisions. They use the property that pixels from closer objects tend to move faster, so that the robot steers

to the side with smaller optical flow. Although this rule seems direct and intuitive, the underlying assumption is oversimplified and may not hold in complex dynamics scenes. Traditional dense optical flow estimation can be achieved by optimization [23] with smoothness constraints, which takes several minutes to compute on a single image pair. Recently, some learning-based methods based on neural networks [24] have been designed to estimate the optical flow with accuracy comparable to traditional methods, while running an order of magnitude faster. In our method, we use FlowNet2 [24] to estimate the motion between two frames.

State-of-the-art detection methods like [25] and [26] can detect different categories of objects and compute their bounding boxes. These learning-based methods can predict with high efficiency and accuracy. In order to estimate the motion with dense optical flows, we need to segment the objects from the background. Mask-RCNN [27] and YOLO [28] are able to compute pixel-level segmentation of different objects.

Lidar sensors can exhibit good performance in terms of computing distances[29], and cameras are widely used for detection[28]. The combination of these two sensors has been used for navigation and autonomous driving [30]. Many works fuse data from Lidar and cameras [31], [32]. In our method, we combine 2D data from Lidar with detected objects from images to compute the obstacles' relative positions and velocities.

III. OVERVIEW

TABLE I. Notation and symbols used in our approach.

Notation	Defination
I	Image captured from the RGB camera
D	Depth map converted from Lidar data
O	Optical flow estimation
M_i	Segmentation mask of the i_{th} obstacle
v_r, v_o	Velocity of the robot and obstacles
p_r, p_o	Position of the robots or obstacles
v_{pref}	Preferred velocity of robot
v_{out}	The output velocity from our method
v_{vo}	The output of OF-VO before using dynamic constraint
$V_{r o}^T$	Veclocity obstacle of robot r caused by obstacle o in step-time T
V_r^T	Total available velocity set
V_a	Allowed velocity space
V_c	Velocity space under constraints of partial observation
c_x, c_y, f_x, f_y	Principal point and focal lengths
t_0, t_1	Time stamp of the last and current frames
T	time step
r_r, r_o	radius of robot and obstacle
s_i, s_r	shape of i_{th} obstacle or robot

Our approach is designed for non-holonomic robots that can be driven by linear and angular velocities. During each timestep, the robot knows the relative position of its target/goal and needs to navigate to the target in an environment with both static and dynamic obstacles. Each obstacle has a velocity v_i at position p_i and all the perceived information may have inaccuracies. Dynamic obstacles typically correspond to moving pedestrians. On the way to the goal, the

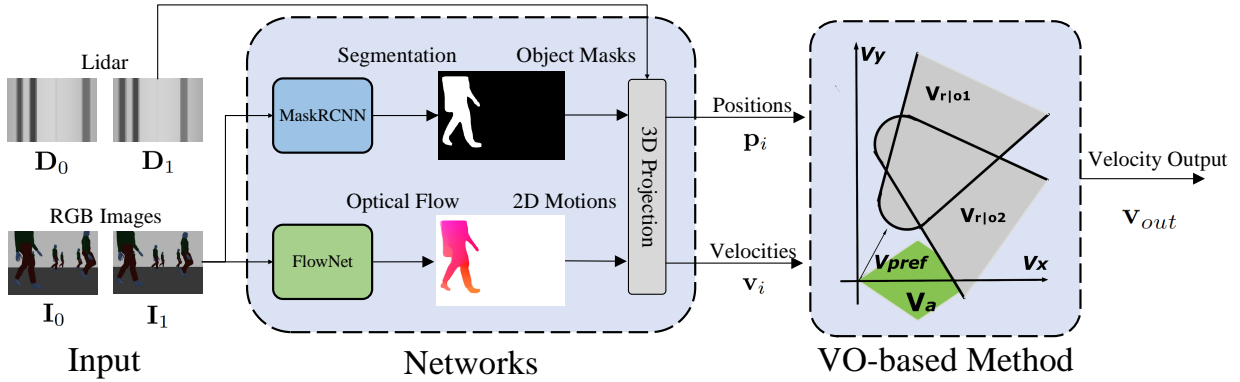


Fig. 2. OF-VO Pipeline: During each time step, our method first takes as input a pair of RGB images and lidar sequences. The optical flow and segmentation masks are computed using FlowNet and MaskRCNN, respectively. Using lidar data and intrinsic camera parameters, our 3D projection module computes the positions and velocities from the masks and optical flow. Due to the limitation of the camera’s FOV, 2D lidar data is also collected to enhance the position estimation. Our method uses a modified velocity obstacles approach to compute a collision-free velocity for the robot that accounts for sensor errors. Before sending the control signals to the robot, a differential driving formulation is used to satisfy the kinematic constraints of the robot.

robot can perceive surrounding obstacles by using a 2D Lidar and an RGB camera to avoid potential collisions. Figure 2 shows the pipeline of our approach, OF-VO. Notations and symbols are summarized in Table I.

We extract the velocities and positions of surrounding obstacles from Lidar data and RGB images, with the help of optical flow estimation and object detection. After that, noises from the perception models are explicitly analyzed, which improves the overall accuracy of our approach. With the position and velocities, \mathbf{p}_o , \mathbf{v}_o , of detected obstacles, our method uses a modified VO-based algorithm to navigate the robot. Real-world scenarios inevitably have inaccuracies and occlusions and only partial observations from the environment due to limited FOV.

For all obstacles detected by the perception model, we model the inaccuracies in detection as Gaussian distributions. Based on the prior approaches [11], [33] our algorithm can provide a tighter bound of probabilistic properties. For unobserved or partially observed objects, we apply non-holonomic or other kinematics to estimate the feasible velocity space of the robot, as described in Section V. Our integrated approach consists of two parts, learning-based perception, and model-based collision avoidance, which are strongly coupled. The hyperparameters in VO algorithm are modified according to different bounds on robot’s velocities or different requirements in terms of confidence in probabilistic collision avoidance.

IV. PERCEPTION

In our approach, we use two commodity visual sensors including an RGB camera and a 2D Hokuyo Lidar. We choose to use these two commodity sensors because the RGB camera is good at perceiving detailed information in the scene, while a 2D Lidar can accurately detect distances of nearby objects. The input to our perception module is a pair of consecutive RGB frames and Lidar data, and the output is the estimated positions \mathbf{p}_o and velocities \mathbf{v}_o of the nearby obstacles. Our algorithm builds on recent learning-based computer vision methods. In our method, an optical

flow network FlowNet [24] and a segmentation network MaskRCNN [27] are used to perceive the objects’ velocities and positions. The input to the neural networks are a pair of images, and we compute the positions and velocities of objects appearing in the images.

At each time step, we need two consecutive frames to calculate the instantaneous velocities. Assume that the current time step is t_1 and the previous time step is $t_0 < t_1$. From the RGB camera we have two pairs of RGB images $\mathbf{I}_{t_1}, \mathbf{I}_{t_0} \in \mathbb{R}^{h \times w \times 3}$, where h, w is the height and width of the images in pixels. For simplicity, we omit t in the subscripts. The input to the FlowNet is the RGB pair $\mathbf{I}_1, \mathbf{I}_0$, and the output is the optical flow $\mathbf{O} \in \mathbb{R}^{h \times w \times 2}$, which represents the displacement of pixels in the 2D images. Therefore, one pixel $\mathbf{s}_1 = [x_1, y_1]$ in \mathbf{I}_1 corresponds to $\mathbf{s}_0 = [x_0, y_0] = [x_1 + \mathbf{O}(x_1, y_1, 1), y_1 + \mathbf{O}(x_1, y_1, 2)]$ in \mathbf{I}_0 . Assume the Lidar sequence is $\mathbf{L} = [l_1, l_2, \dots, l_k]$, where l_i is the distance to the nearest point at angle θ_i . The positions of those points in the horizontal plane can then be computed by $(l \sin \theta, l \cos \theta)$, and projected into the image space as a depth image \mathbf{D} . The depth \mathbf{D}'_0 and position SS'_0 of pixels in the \mathbf{I}_1 frame at t_0 time can be computed using optical flow warping [24].

The next step is to separate moving obstacles, like pedestrians, from the raw image such that we can compute their positions and velocities. We feed image \mathbf{I}_1 to another segmentation network MaskRCNN to estimate pixel-level segmentations. Assume that for an object i , MaskRCNN predicts its segmentation mask $\mathbf{M}_i \in \{0, 1\}^{h \times w}$. The depth d_i and the position $\mathbf{s}_i = (x_i, y_i)$ in the image space of an object can be calculated as the weighted mean in the masked area. Let the camera have principal point $[c_x, c_y]$ and focal lengths (f_x, f_y) , the 3D position of the object can be computed by $\mathbf{p}_i = [(x_i \cdot d_i - c_x \cdot d_i) / f_x, (y_i \cdot d_i - c_y \cdot d_i) / f_y, d_i]$. After that, the relative velocities in the robot frame can be easily computed by $\bar{v}v_i = (\mathbf{p}_{1i} - \mathbf{p}_{0i}) / (t_1 - t_0)$. The corresponding absolute velocities \mathbf{v}_i can be computed from $\bar{v}v_i$ and the robot’s velocities at this time. Moreover, the

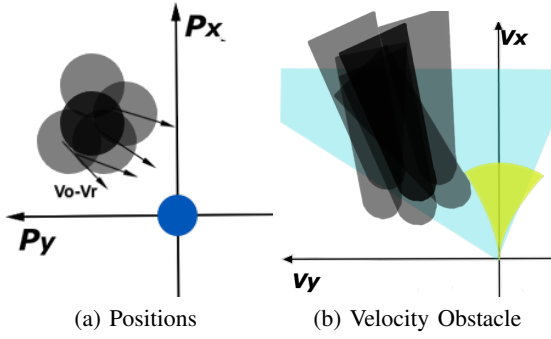


Fig. 3. Modified Velocity Obstacles with Partial Observation of obstacles: (a) In a given frame, where the robot is at the origin with radius r_r and velocity \mathbf{v}_r . Given an obstacle at position \mathbf{p}_o with velocity \mathbf{v}_o . The black area is computed from the position of obstacle and its radius is $r_r + r_o$, and relative velocity between the robot and the obstacle is $\mathbf{v}_o - \mathbf{v}_r$ (i.e., the Minkowski sum). Considering the inaccuracies of positions and velocities of obstacles, the gray areas represent the Minkowski sums with different possible positions and the arrows correspond to different possible relative velocities between the obstacle and the robot. (b) shows the velocity space of the robot, where gray regions represent different possible velocity obstacles corresponding to the obstacle positions in (a); blue region is the region corresponding to the field of view; and yellow region corresponds to the limitations on the velocities from the kinematic constraints of the robot.

size of moving obstacles appearing in the image can be estimated from the bounding box estimated using MaskRCNN. Lidar data can further compute the radius of obstacles that are outside the camera's FOV. Compared to tracking-based velocity estimation, our method utilizes pixel-level motion information. Thus, our approach does not suffer from correspondence or loss of tracking target. Moreover, our FlowNet and MaskRCNN can take advantage of pre-trained models, which are trained on large-volume datasets and are able to generalize well to the real world.

V. COLLISION AVOIDANCE

After detection of nearby obstacles using our perception algorithm, we use a modified Velocity-Obstacle(VO) algorithm for collision avoidance. In this section, we present our collision avoidance algorithm. Moreover, we address the issue of handling partial observations and kinematic constraints of the robot.

The velocity obstacle algorithm is widely used for collision avoidance in dynamic environment. This algorithm calculates relative positions and velocities of nearby obstacles and finds a feasible subset of velocities in which the robot can move. The input of our VO-based algorithm includes probabilistic velocities and positions of obstacles computed from the perception modules, the velocity of the robot and its relative goal location.

In our model, the largest robot's field of view is limited by the field of view of 2D lidar. For areas inside the range of the camera, the VO algorithm [3] is directly used based on the information about detected obstacles, as shown in Fig. 3. (a) represents the configuration where the robot deals with the obstacle at \mathbf{p}_o . The obstacle has a radius r_o and a velocity \mathbf{v}_o , which we assume does not during time step of length T , and the robot has radius r_r and velocity \mathbf{v}_r . When we treat the robot as a point, the Minkowski sum of the obstacle and

the robot has the radius of $r_r + r_o$, and the relative velocity is $\mathbf{v}_o - \mathbf{v}_r$. Because of the inaccuracies in detection, the position of each obstacle can be modeled as a distribution around the perceived location. The gray circles in figure 3(a) represent the possible locations of the obstacle and the arrows show the possible relative velocity of the robot. To avoid a collision during time step T , the robot cannot choose velocities in the middle black area in Fig.3 (b), which is the velocity obstacle $V_{r|o_1}^T$ of robot r due to the obstacle o_1 . The gray areas near the black area are possible velocity obstacles, each corresponding to the inaccurate position and velocity of the robot. A velocity obstacle is defined in Equation 1:

$$V_{r|o}^T = \{\mathbf{v} | \exists t \in [0, T] :: t\mathbf{v} \in D(\mathbf{p}_o - \mathbf{p}_r, r_r + r_o)\} \quad (1)$$

$$D(\mathbf{p}, r) = \{\mathbf{q} | \|\mathbf{q} - \mathbf{p}\| < r\},$$

where D is the circular disk centered at position P with radius r .

Since the FOV of the camera is smaller than the Lidar, dynamic obstacles may appear in the detection area of this lidar but not of the RGB camera. As a result, the velocities of such obstacles are unknown and there is a potential collision during the time step T . We use additional constraints to prevent such collisions. Our approach considers two types of dynamic obstacles: robotic obstacles and pedestrian obstacles. The robotic obstacles have the same configurations as the robot, and pedestrian obstacles correspond to moving pedestrians or other dynamic objects etc.

For robotic obstacles, it follows that the robots will not collide with obstacles within the detection area of the camera. As a result, if we choose the velocity within the field of view of the camera, then the robots will not collide with each other. This can be expressed as:

$$V_c = \left\{ (v_x, v_y) \mid \left| \arctan\left(\frac{v_x}{v_y}\right) \right| < \frac{FOV_c}{2} \right\}. \quad (2)$$

where FOV_c is the field of view of the camera, and v_x, v_y are in the frame of the robot.

For pedestrian-obstacles, we assume that each obstacle is going to maintain its original speed. At position \mathbf{p}_i and at current time-step, let's assume that the obstacle has velocity \mathbf{v}_i . Let the maximum velocity of the pedestrian-obstacle is $\|\mathbf{v}_o\| = 1.5m/s$, which is the average speed of pedestrians [34]. Given this assumption, if the robot can maintain sufficient distance from the obstacle during the next time step, it will not collide with the obstacle. A velocity $\mathbf{v}_r = (x_r, y_r)$ having a maximum of $\|\mathbf{v}_r\| = 1m/s$ is used in our formulation in the Equation 3.

$$V_{r|l}^T = \{\mathbf{v} | \|\mathbf{v}_r * t - \mathbf{p}_o\| > C_t\}, \text{ for all } t \in (0, T], \quad (3)$$

where C_t is the threshold of collision, which is the minimum distance between the obstacle and the robot. T is the duration of the time-step.

All these constraints from the obstacles are taken into account in Equation V, where $\hat{V}_{r|o_i}^T$ is the complementary set of $V_{r|o_i}^T$. We assume that there are m obstacles in the

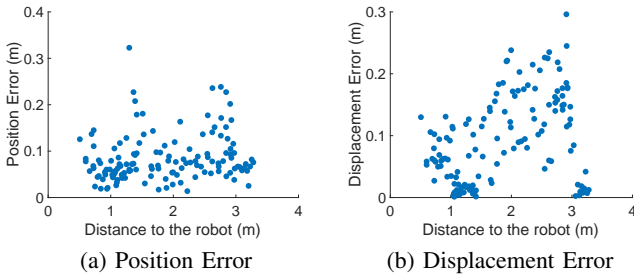


Fig. 4. Error in distance and displacement estimation: (a) shows that the errors in position estimation are distributed uniformly along the obstacles’ distance. (b) shows that the errors in displacement estimation increase with the distance. The estimation has the highest accuracy at 1 meter distance.

detecting range of the camera and n obstacles out of the camera’s view but inside the view of the lidar.

$$V_r^T = \left\{ V_c \cap V_{l_i} \cap \hat{V}_{r|o_j}^T \mid i \in [1, 2, \dots, n], j \in [1, 2, \dots, m] \right\}. \quad (4)$$

This formulation of velocity computation assumes accurate location of the obstacles. In Section VI, we present a probabilistic formulation that takes into sensor errors.

A. Kinematic Constraints

Our approach can handle kinematic and non-holonomic constraints. The output of our velocity obstacle algorithm is computed in Euclidean coordinates. In order to satisfy the kinematic constraints of the robot, we convert the constraints on the linear and angular velocities of the robot to the Euclidean space. This constraint is shown as the yellow area in Figure 3(b).

Let \mathcal{D} denote the area of constraint from kinematic relations, now the total constraint can be represented as $\mathcal{C} = V_r^T \cap \mathcal{D}$. For each step, the robot has a preferred velocity of \mathbf{v}_{pref} , which is calculated according to its current position and goal position[4].

$$L = \arg \min_{\mathbf{v}} \|\mathbf{v} - \mathbf{v}_{pref}\|, \quad \mathbf{v} \in \mathcal{C} \quad (5)$$

VI. ERROR ANALYSIS AND PROBABILISTIC COLLISION AVOIDANCE

In this section, we analyze the error from our perception algorithm and use that to formulate our probabilistic collision avoidance algorithm

We estimate the position and displacement of obstacles between consecutive frames. The velocities of obstacles can be computed by the displacement, robot velocities, and time steps. We plot the L2 error of estimations in Figure 4. The results indicate that the displacement (velocity) estimation is more accurate for nearby obstacles, and the inaccuracy in position estimation increases based on the distance from the robot.

We analyze the accuracy of the two networks used in our perception algorithm. As reported by FlowNet2 [24], the average endpoint error in KITTI 2012 is $e_f = 4.09$, which means that predicted optical flows are 4.09 pixels away from the ground truth (on average). For an object whose depth

is z , an error of e_f pixels in optical flow would result in an error of $e_f \cdot z/f$ to its displacement estimation. In our implementation, we have $f_x = f_y = 457$, so the error for an object at $2m$ away would be $0.02m$. The error of *SegNet* is harder to quantify. From Figure 1, we can see that the segmentation of the pedestrian is reasonably good in our benchmarks. The average precision (.50 IoU) of MaskRCNN is 62.3% [27] on the COCO dataset [35], which means nearly two-thirds of predictions have more than .50 IoU. In order to make our collision avoidance more conservative, we enlarge the bounding box of moving obstacles by more than 50%. Based on the analysis of these inaccuracies, we assume the obstacles near the robots have probabilistic positions and velocities

A. Probabilistic Collision Avoidance

In this section, we account for the sensor errors and derive bounds for probabilistic collision avoidance. We model obstacles’ parameters as Gaussian distributions and get the velocity constraint for the robot. Then we give a parameter k in Lemma 1.1, which represents a confidence in collision avoidance. Our bound derivation makes some assumptions on the dynamic obstacles. We assume that a moving agent would slow down if it moves close to the robot. Moreover, a moving agent would prevent collision if it is behind the robot.

Because of the inaccuracies of sensors and also uncertainties in complex real-world situations, we assume the observed obstacles have errors in positions and velocities with different probabilities. In our algorithm, we compute the best velocity based on the positions and velocities of obstacles, so we only need to model these values (see Equation 7). In our formulation they are represented by Gaussian distributions, as shown in Figure 3. We assume each vector is isotropic in all directions, where elements in the same vector are independent and their variances have the same relationship with distance:

$$\mathbf{p}_i \approx \mathcal{N}_2(\mu_p, \Sigma_p(d)) \quad (6)$$

$$\mathbf{v}_i \approx \mathcal{N}_2(\mu_v, \Sigma_v(d)), \mathbf{v}_r \approx \mathcal{N}_2(\mu_r, \Sigma_r) \quad (7)$$

where \mathbf{p}_i is the relative position of the i_{th} obstacle to the robot; \mathbf{v}_i is the velocity of the i_{th} obstacle; d is the distance between the obstacle and the robot, and \mathbf{v}_r is the velocity of the robot. If the obstacle is nearer, it results in more accurate perception of positions and velocities of obstacles. Based on the formulation, $\Sigma_v(d) = \sigma_v(d)^2 \mathbf{I}$ and $\Sigma_p(d) = \sigma_p(d)^2 \mathbf{I}$, we find that $\sigma_v(d)^2$ and $\sigma_p(d)^2$ are monotonically decreasing.

For any velocity of the robot, \mathbf{v} and all $t \in (0, T]$, the $\hat{V}_{r|o}^T$ and Equation 3 can be rewritten as Equation 8:

$$f_i(\mathbf{v}, t | \mathbf{p}_i, \mathbf{v}_i) = \|\mathbf{p}_i - (\mathbf{v} - \mathbf{v}_i)t\|^2 - (r_r + r_i)^2 > 0 \quad (8)$$

where r_r and r_i are the radius of the robot and the obstacle i , respectively. \mathbf{v} and \mathbf{v}_i represents the traveling distance of the robot and the i_{th} obstacle at given time t , respectively. This equation ensures that the distance between the robot

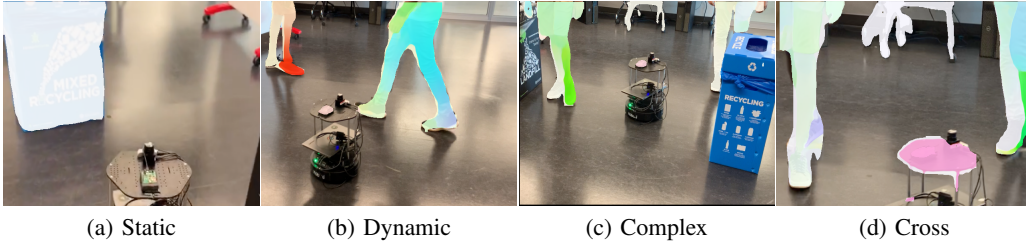


Fig. 5. Navigation across a room with different configurations: Our algorithm running on Turtlebot2 is used to navigate the robot and avoid collisions with the pedestrians and obstacles. Our algorithm can compute collision free trajectories for the robot in these scenarios with static obstacles and multiple moving pedestrians.

and the obstacle during the next time step is larger than sum of their radius.

Theorem 6.1: For any velocity \mathbf{v} of the robot, the probability of f_i , $Prob(f_i(\mathbf{v}|\mathbf{p}_i, \mathbf{v}_i))$ is a non-central χ^2 distribution with different σ , where the mean is a function of \mathbf{v} and variance with regards to d is monotonically decreasing, where d is the distance from the obstacle to the robot and is determined when obstacle is detected.

Proof: Let us denote $p_i = (x_i^p, y_i^p)$ with mean (μ_x^p, μ_y^p) and variance $\sigma_p(d)^2\mathbf{I}$; $v_i = (x_i^v, y_i^v)$ with mean (μ_x^v, μ_y^v) and variance $\sigma_v(d)^2\mathbf{I}$ and $\mathbf{v} = (v_x^r, v_y^r)$. Because \mathbf{p}_i and \mathbf{v}_i are all isotropic, we have $\mathbf{d}_{rel}(x, y)$ as the distribution of calculated points with mean μ_{rel} and variance $\Sigma_{rel}(d)$:

$$\mathbf{d}_{rel}(x, y) = Prob(\mathbf{p}_i - \mathbf{v}t + \mathbf{v}_i t) \approx \mathcal{N}(\mu_{rel}, \Sigma_{rel}(d)) \quad (9)$$

$$\mu_{rel} = (\mu_{rel}^x, \mu_{rel}^y) = (\mu_x^p + \mu_x^v t - v_x^r t, \mu_y^p + \mu_y^v t - v_y^r t) \quad (10)$$

$$\Sigma_{rel}(d) = (\sigma_p(d)^2 + \sigma_v(d)^2 t^2)\mathbf{I} \quad (11)$$

According to non-central chi-squared distribution, the distribution of l_2 norm of d_{rel} is represented as $\mathcal{X}_2(v|\mathbf{p}_i, \mathbf{v}_i)$ and d is the detected distance of the obstacle:

$$\mu_{norm} = 2 + (\mu_{rel}^x)^2 + (\mu_{rel}^y)^2 = k(v) \quad (12)$$

$$\sigma_{norm} = 4(\sigma_p(d)^2 + \sigma_v(d)^2 t^2)(1 + (\mu_{rel}^x)^2 + (\mu_{rel}^y)^2) = g(d). \quad (13)$$

We denote $\mu_f(\mathbf{v}) = \mu_{norm} - (r_r + r_i)^2$ and $\sigma_f(d) = g(d)$. According to Equation 13, since $\sigma_p(d)^2$ and $\sigma_v(d)^2$ are all monotonically decreasing w.r.t. d , the variance of f_i is also monotonically decreasing. ■

Theorem 6.1 illustrates the type of constraint on the velocity obstacle formulation based on one dynamic obstacle. This is the basic constraint on the possible robot velocities that are used to avoid this obstacle. Based on this constraint, we give a confidence value in Lemma 1.1 to choose velocities for different probabilities of collision avoidance.

Since the variables in Equation 8 are all random variables, in order to constraint the probability of collision, we use chance constraint w.r.t the variants in Equation 8 as $P(f_i(\mathbf{v}, t|\mathbf{p}_i, \mathbf{v}_i) > 0)$ with given t . $P(f_i(\mathbf{v}|\mathbf{p}_i, \mathbf{v}_i, t) > 0)$ is a function of \mathbf{v} , \mathbf{p} and \mathbf{v}_i , we denote it as $P(\mathbf{v}|\mathbf{p}_i, \mathbf{v}_i, t)$.

Lemma 1.1: Given a scalar value $k > 0$, the chance constraint $P(\mathbf{v}|\mathbf{p}_i, \mathbf{v}_i, t)$ is bounded by $\frac{4}{9k^2}$.

Proof: In order to satisfy the constraint function, $P(f_i(\mathbf{v}|\mathbf{p}_i, \mathbf{v}_i, t) > 0)$, we can give a bound to function

f_i to constraint the random variable to be positive, then we have:

$$(X - \mu_f) - k|\sigma_f| > 0 \quad (14)$$

According to Vysochanskij–Petunin inequality, we have:

$$P(f_i(\mathbf{v}|\mathbf{p}_i, \mathbf{v}_i, t) > 0) > \frac{4}{9k^2} \quad (15)$$

Lemma 1.1 shows that given t , when we choose the area with the bound of $(\mu_f - k\sigma_f, \mu_f + k\sigma_f)$, we have a confidence larger than $\frac{4}{9k^2}$, that will satisfy Equation 8. In order to guarantee collision avoidance with the obstacles, we need to make sure that when robot is moving it will not result in a collision. For all time $t \in (0, T]$, the robot's velocity need to always satisfy $P(f_i(\mathbf{v}|\mathbf{p}_i, \mathbf{v}_i, t) > 0) > \frac{4}{9k^2}$. We also give a constraint on T based on Theorem 6.2:

Theorem 6.2: When a time step $T > \frac{\mathbf{p}_i \cdot (\mathbf{v} - \mathbf{v}_i)}{\|\mathbf{v} - \mathbf{v}_i\|^2} > 0$ the robot's velocity should also satisfy the constraint in [11].

Proof: Assume a given velocity \mathbf{v} , the relative velocity is $\mathbf{v}_l = \mathbf{v} - \mathbf{v}_i = (v_x, v_y)$. $\mathbf{p} = (p_x, p_y)$ is the relative position of obstacle i . $r = r_r + r_i$ is the sum of the radius of robot and obstacle i . Then we have :

$$\begin{aligned} f_i(t|\mathbf{v}, \mathbf{v}_i, \mathbf{p}_i) &= \|\mathbf{p}_i - \mathbf{v}_l t\|^2 - (r_r + r_i)^2, \\ f_i(t|\mathbf{v}, \mathbf{v}_i, \mathbf{p}_i) &= (p_x - v_x t)^2 + (p_y - v_y t)^2 - r^2, \\ f_i(t|\mathbf{v}, \mathbf{v}_i, \mathbf{p}_i) &= (v_x^2 + v_y^2)t^2 - 2(p_x v_x + p_y v_y)t, \\ &\quad + (p_x^2 + p_y^2 - r^2). \end{aligned} \quad (16)$$

Given a time step T , $t \in (0, T]$. We denote $f_i(t|\mathbf{v}, \mathbf{v}_i, \mathbf{p}_i) = at^2 + bt + c$ where $a > 0$. If $t = \max(-\frac{b}{2a}, 0)$ and $f_i(t|\mathbf{v}, \mathbf{v}_i, \mathbf{p}_i) > 0$, we can guarantee that the constraint $f_i(t|\mathbf{v}, \mathbf{v}_i, \mathbf{p}_i) > 0$. When $-\frac{b}{2a} < 0$ or $0 < t < -\frac{b}{2a}$, we have satisfied this constraint by lemma 1.1. When $0 < -\frac{b}{2a} < t$, we have:

$$\begin{aligned} (v_x^2 + v_y^2)t^2 - 2(p_x v_x + p_y v_y)t + \\ (p_x^2 + p_y^2 - r^2) &> 0, \\ \frac{(p_x v_x + p_y v_y)^2}{v_x^2 + v_y^2} - \frac{2(p_x v_x + p_y v_y)^2}{v_x^2 + v_y^2} \\ + (p_x^2 + p_y^2 - r^2) &> 0, \\ \frac{(p_x v_x + p_y v_y)^2}{v_x^2 + v_y^2} - (p_x^2 + p_y^2 - r^2) &< 0. \end{aligned} \quad (17)$$

Equation 17 is the constraint used in [11]. ■

Proof of the theorem is given in [36]. According to Theorem 6.2, when we choose $T < \frac{\mathbf{p}_i \cdot (\mathbf{v} - \mathbf{v}_i)}{\|\mathbf{v} - \mathbf{v}_i\|^2}$, we need to use constraint of Lemma 1.1. However, when $T \leq \frac{\mathbf{p}_i \cdot (\mathbf{v} - \mathbf{v}_i)}{\|\mathbf{v} - \mathbf{v}_i\|^2}$, constraints in [11] need to be satisfied. After we have constrained T , we also restrict the area of possible velocities to choose. In this manner, we can combine the constraints caused by all nearby obstacles together. We use the function, $g(\mathbf{p}_i, \mathbf{v}_i, T)$, to represent the allowable velocity area related to the obstacle i . For all obstacles detected, denoted as set C_o , with different distances to the robot, we approximate the distribution of all allowable velocities as the sum of multiple distributions weighted by function $f(d)$. This function monotonically decreases when d increases:

$$\int_{d \in \mathcal{D}} f(d) = 1, \quad \mathcal{G} = \bigcap_{i \in C_o} f(d)g(\mathbf{p}_i, \mathbf{v}_i), \quad (18)$$

where \mathcal{D} is the range of detection $[0.1, 10]$. Then the Equation V can be rewritten as:

$$V_r^T = V_c \bigcap \mathcal{G}. \quad (19)$$

We use Theorem 6.2 and Lemma 1.1 to set the time step value and confidence in the collision avoidance algorithm given in Section V. Based on the parameters, Equation 19, V_r^T corresponds to the feasible velocity space that takes all the obstacles into account. Overall, Equation 19 gives guarantee of at least $\frac{4}{9k^2}$ probability to avoid the obstacles. Combined with kinematic constraints \mathcal{D} we can choose best velocity using Equation 5.

VII. EXPERIMENTS AND RESULTS

In this section, we describe the implementation details and highlight the performance in real-world and simulated scenarios. We also show the improvement in the performance of our approach in scenarios with partial observations.

A. Experimental Setup

In the implementation, we use Turtlebot2 as the robot platform, Astra RGB camera and Hokuyo Lidar. The resolution of the RGB camera is 640×480 , and 520 range data for Lidar. We gathered sensor inputs and generated results on a laptop with an Intel i7-9750H CPU (2.6 GHz) with 32 GB memory and an Nvidia GeForce RTX 2070 GPU.

B. Simulation and Real-world Scenarios Used for Testing

We run our system with Ubuntu 18.04, ROS Melodic, and PyTorch 1.4. The segmentation network (SegNet) is mask-RCNN from detectron2 [37] trained on the COCO dataset [35] and the optical flow (OFNet) network is FlowNet2 [24] trained on FlyingChairs [38] and FlyingThings3D [39]. These datasets contains large amount of real and synthetic data, which enables our networks to generalize well to the data captured in simulated and real-world environments.

In the real world scenarios, we use Turtlebot with Pozyx system as localization method. Figure 5 shows a Turtlebot2 with our algorithm moving in four real-world scenarios, where pedestrians are (a) standing still, (b) moving towards

the robot, (c) moving between obstacles, (d) and move in a perpendicular direction.

In the simulation, we use Gazebo 9.0.0 to build environments. In order to test the performance of our method, we created different scenarios(as shown in Figure 6) to detail the improvement brought by using different sub-models of the method and the performances of different algorithms are in Table VII-C.

1. **Empty** (Figure 6(a)): In this scenario, OF-VO tested with random goal and start position. It is used to test if the robot has the basic functionality to go to the goal position.

2. **Static** (Figure 6(b)): This scenarios requires robot to go around static obstacles and go to the goal position.

3. **Dynamic** (Figure 6(c)): In this scenario, there is a crowd of people moving towards the robot from the front. The robot needs to avoid pedestrians and find its way to the goal position.

4. **Complex** (Figure 6(d)): In this scenario there are not only static but also dynamic obstacles. A robot is required to be able to avoid both types of obstacles.

5. **Cross** (Figure 6(e)): In this scenario, pedestrians are moving toward the robot from the side. This scenario requires the ability to avoid dynamic obstacles from both sides and challenging in terms of perception issues.

C. Partial-Observation Based Probabilistic VO

In our approach, because of the limitation of sensors, we have only partial observations around the robot. In order to compare the performance of our new method with the original VO method [3], we tested OF-VO in scenarios with pedestrians going across from outside of the view of the camera, as shown in Figure 6(e). Because of the inaccuracies in perception, the detected positions and velocities of obstacles around the robot are treated as Gaussian distributions. The available velocity area of the robot in each step is a combination of non-Gaussian distributions. Our algorithm chooses the best velocity from the combination of distributions with different constraints. In order to compare the performance of different confidences in collision avoidance, we tested the robot with different confidence parameters in different scenarios. The successful rate using our approach is 89%. However, without the constraints, the success rate drops to around 60%. The performance of our algorithm improves by 33% in dynamic scenes, where pedestrians may walk towards the robot from outside the field-of-view of the camera.

D. Performance: Local Navigation

We compare our algorithm (OF-VO) with two other collision avoidance methods, the Dynamic-Window Approach (DWA) and another Deep Reinforcement Learning-based (DRL) approach[12]. We compare these three algorithms using three criteria:

Trajectory Length: This value gives information about the performance of each algorithm, the shortest length has better accuracy in terms of path calculation and perception.

Navigation Time: The value shows how long each algorithm takes to navigate the robot towards the goal. It gives

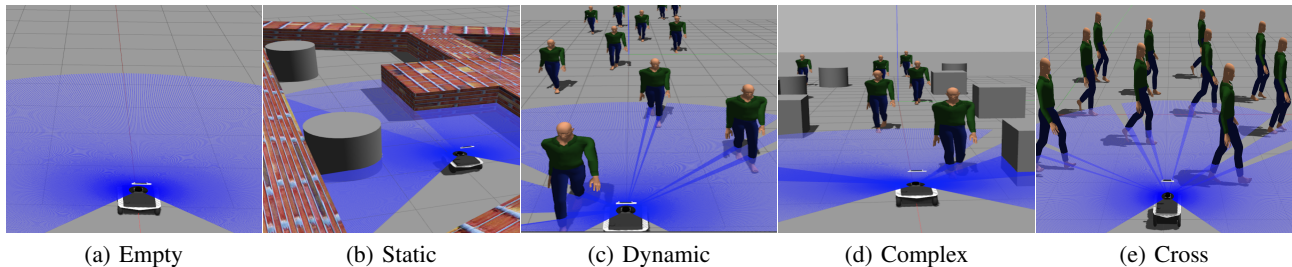


Fig. 6. Simulation Scenarios: We use five scenes to run the comparison and ablation study. The scenes corresponding to (c), (d) and (e) are dynamic scenes with multiple pedestrians. The robot goes from a start point to a goal point, while avoiding dynamic and static obstacles.

Scenarios	Trajectory length (m)			Navigation Time (sec)			Success Rate (%)		
	OF-VO	DWA	DRL	OF-VO	DWA	DRL	OF-VO	DWA	DRL
Empty	10.8	5.80	6.05	15.7	14.6	24.9	100	100	100
Static obstacles	11.4	18.16	9.9	30.08	15.6	19.11	100	95	90
Dynamic obstacles	42.5	29.98	42.19	53.17	42.93	43.6	90	20	55
Cross Scenario	14.53	N/A	14.3	27.8	N/A	10.0	80	N/A	20

TABLE II. We compare OF-VO with DWA [2] and DRL methods [12] in terms of accuracy, speed, and reliability in the simulated scenarios (Fig. 6). OF-VO has the highest success rate, especially in the highly dynamic environments, including dynamics obstacles and cross scenarios. DWA and DRL result in collisions with the pedestrians, when the density and velocity of the pedestrians increases.

Successful Rate	k=0.1	k=0.5	k=0.7	k=1
Static obstacles	100	100	100	100
Dynamic obstacles	60	65	76	90
Cross obstacles	16	36	64	80

TABLE III. Quantitative comparison with different values of confidences in probabilistic collision avoidance. With higher k , the confidence is higher and navigation method tends to be more conservative.

information about the processing speed and the timestep used for navigation.

Success Rate: This value shows the overall performance in terms of collision avoidance and safety.

Results in Figure VII-C indicate that our method has the highest success rate in terms of avoiding collisions. In highly dynamic scenarios, DWA and DRL will easily collide with pedestrians. Our robot can successfully avoid obstacles by using our probabilistic collision avoidance scheme. Since our method chooses more conservative strategies to avoid collisions, it also takes more time and distance to navigate towards the goal.

VIII. CONCLUSIONS AND LIMITATIONS

In this paper, we present a hybrid navigation algorithm that combines learning-based perception and model-based collision avoidance. We have implemented OF-VO on a Turtlebot with commodity visual sensors, including an RGB camera and a lidar. We have evaluated the performance in complex dynamic scenes with multiple pedestrians and highlight the benefits over prior model-based (DWA) and learning-based (DRL) methods in terms of success rate and reliability.

Although our method performs well in general, it has some limitations. In particular, the Velocity-Obstacle is a local

navigation method and the robot is constrained so that it does not move backward or backtracks. As a result, the robot may get stuck in an impasse, where there is no feasible velocity (i.e. freezing behavior). Moreover, the optical flow estimation has lower performance for large displacements. We currently model the sensor errors using simple Gaussian mixture model formulation, though it can be extended to other non-Gaussian noise distributions [40]. Our formulation can be conservative. Moreover, if there are fast-moving obstacles outside the field-of-view of the camera, they can result in collisions. As part of future work, we would like to overcome these limitations and combine our work with global navigation methods. We would like to evaluate the performance of different robots in complex and outdoor scenes.

IX. ACKNOWLEDGEMENTS

This work was supported in part by ARO Grants W911NF1910069 and W911NF1910315, Semiconductor Research Corporation (SRC), and Intel.

REFERENCES

- [1] H. Ma, S. Koenig, N. Ayanian, L. Cohen, W. Hönig, T. Kumar, T. Uras, H. Xu, C. Tovey, and G. Sharon, "Overview: Generalizations of multi-agent path finding to real-world scenarios," *arXiv preprint arXiv:1702.05515*, 2017.
- [2] D. Fox, W. Burgard, and S. Thrun, "The dynamic window approach to collision avoidance," *IEEE Robotics & Automation Magazine*, vol. 4, no. 1, pp. 23–33, 1997.
- [3] P. Fiorini and Z. Shiller, "Motion planning in dynamic environments using velocity obstacles," *The International Journal of Robotics Research*, vol. 17, no. 7, pp. 760–772, 1998.
- [4] J. Van Den Berg, S. J. Guy, M. Lin, and D. Manocha, "Reciprocal n-body collision avoidance," in *Robotics research*. Springer, 2011, pp. 3–19.
- [5] A. Levy, C. Keitel, S. Engel, and J. McLurkin, "The extended velocity obstacle and applying orca in the real world," in *2015 IEEE International Conference on Robotics and Automation (ICRA)*. IEEE, 2015, pp. 16–22.

- [6] M. Li, R. Jiang, S. S. Ge, and T. H. Lee, "Role playing learning for socially concomitant mobile robot navigation," *CAAI Transactions on Intelligence Technology*, vol. 3, no. 1, pp. 49–58, 2018.
- [7] A. Pfrunder, P. V. Borges, A. R. Romero, G. Catt, and A. Elfes, "Real-time autonomous ground vehicle navigation in heterogeneous environments using a 3d lidar," in *2017 IEEE/RSJ International Conference on Intelligent Robots and Systems (IROS)*. IEEE, 2017, pp. 2601–2608.
- [8] A. J. Sathyamoorthy, J. Liang, U. Patel, T. Guan, R. Chandra, and D. Manocha, "Densecavoid: Real-time navigation in dense crowds using anticipatory behaviors," *arXiv preprint arXiv:2002.03038*, 2020.
- [9] M. Pfeiffer, M. Schaeuble, J. Nieto, R. Siegwart, and C. Cadena, "From Perception to Decision: A Data-driven Approach to End-to-end Motion Planning for Autonomous Ground Robots," *arXiv e-prints*, p. arXiv:1609.07910, Sep 2016.
- [10] Y. Zhu, R. Mottaghi, E. Kolve, J. J. Lim, A. Gupta, L. Fei-Fei, and A. Farhadi, "Target-driven Visual Navigation in Indoor Scenes using Deep Reinforcement Learning," *arXiv e-prints*, p. arXiv:1609.05143, Sep 2016.
- [11] B. Gopalakrishnan, A. K. Singh, M. Kaushik, K. M. Krishna, and D. Manocha, "Prvo: Probabilistic reciprocal velocity obstacle for multi robot navigation under uncertainty," in *2017 IEEE/RSJ International Conference on Intelligent Robots and Systems (IROS)*, Sep. 2017, pp. 1089–1096.
- [12] T. Fan, P. Long, W. Liu, and J. Pan, "Fully distributed multi-robot collision avoidance via deep reinforcement learning for safe and efficient navigation in complex scenarios," *arXiv preprint arXiv:1808.03841*, 2018.
- [13] H. Bai, S. Cai, N. Ye, D. Hsu, and W. S. Lee, "Intention-aware online pomdp planning for autonomous driving in a crowd," in *2015 IEEE International Conference on Robotics and Automation (ICRA)*, May 2015, pp. 454–460.
- [14] L. Xie, S. Wang, A. Markham, and N. Trigoni, "Towards Monocular Vision based Obstacle Avoidance through Deep Reinforcement Learning," *arXiv e-prints*, p. arXiv:1706.09829, Jun 2017.
- [15] V. Mnih, A. P. Badia, M. Mirza, A. Graves, T. Lillicrap, T. Harley, D. Silver, and K. Kavukcuoglu, "Asynchronous methods for deep reinforcement learning," in *International conference on machine learning*, 2016, pp. 1928–1937.
- [16] J. Schulman, F. Wolski, P. Dhariwal, A. Radford, and O. Klimov, "Proximal policy optimization algorithms," *arXiv preprint arXiv:1707.06347*, 2017.
- [17] D. Wolinski, S. J. Guy, A.-H. Olivier, M. Lin, D. Manocha, and J. Petré, "Parameter estimation and comparative evaluation of crowd simulations," in *Computer Graphics Forum*, vol. 33, no. 2. Wiley Online Library, 2014, pp. 303–312.
- [18] Z. Forootaninia, I. Karamouzas, and R. Narain, "Uncertainty models for ttc-based collision-avoidance." in *Robotics: Science and Systems*, vol. 7, 2017.
- [19] N. E. Du Toit and J. W. Burdick, "Robot motion planning in dynamic, uncertain environments," *IEEE Transactions on Robotics*, vol. 28, no. 1, pp. 101–115, 2011.
- [20] G. Angeris, K. Shah, and M. Schwager, "Fast reciprocal collision avoidance under measurement uncertainty," *arXiv preprint arXiv:1905.12875*, 2019.
- [21] J.-M. Li, C. W. Chen, and T.-H. Cheng, "Estimation and tracking of a moving target by unmanned aerial vehicles," in *2019 American Control Conference (ACC)*. IEEE, 2019, pp. 3944–3949.
- [22] H. Chao, Y. Gu, and M. Napolitano, "A survey of optical flow techniques for robotics navigation applications," *Journal of Intelligent & Robotic Systems*, vol. 73, no. 1-4, pp. 361–372, 2014.
- [23] B. K. Horn and B. G. Schunck, "Determining optical flow," in *Techniques and Applications of Image Understanding*, vol. 281. International Society for Optics and Photonics, 1981, pp. 319–331.
- [24] E. Ilg, N. Mayer, T. Saikia, M. Keuper, A. Dosovitskiy, and T. Brox, "FlowNet 2.0: Evolution of optical flow estimation with deep networks," in *Proceedings of the IEEE conference on computer vision and pattern recognition*, 2017, pp. 2462–2470.
- [25] R. Girshick, J. Donahue, T. Darrell, and J. Malik, "Rich feature hierarchies for accurate object detection and semantic segmentation," in *Computer Vision and Pattern Recognition*, 2014.
- [26] S. Ren, K. He, R. Girshick, and J. Sun, "Faster R-CNN: Towards real-time object detection with region proposal networks," in *Advances in Neural Information Processing Systems (NIPS)*, 2015.
- [27] K. He, G. Gkioxari, P. Dollár, and R. Girshick, "Mask r-cnn," in *Proceedings of the IEEE international conference on computer vision*, 2017, pp. 2961–2969.
- [28] J. Redmon and A. Farhadi, "Yolo9000: better, faster, stronger," in *Proceedings of the IEEE conference on computer vision and pattern recognition*, 2017, pp. 7263–7271.
- [29] P. Wei, L. Cagle, T. Reza, J. Ball, and J. Gafford, "Lidar and camera detection fusion in a real-time industrial multi-sensor collision avoidance system," *Electronics*, vol. 7, no. 6, p. 84, 2018.
- [30] C. Debeunne and D. Vivet, "A review of visual-lidar fusion based simultaneous localization and mapping," *Sensors*, vol. 20, no. 7, p. 2068, 2020.
- [31] G. A. Kumar, J. H. Lee, J. Hwang, J. Park, S. H. Youn, and S. Kwon, "Lidar and camera fusion approach for object distance estimation in self-driving vehicles," *Symmetry*, vol. 12, no. 2, p. 324, 2020.
- [32] A. Ramezani Dooraki and D.-J. Lee, "An end-to-end deep reinforcement learning-based intelligent agent capable of autonomous exploration in unknown environments," *Sensors*, vol. 18, no. 10, p. 3575, 2018.
- [33] J. S. Park, C. Park, and D. Manocha, "Efficient probabilistic collision detection for non-convex shapes," in *2017 IEEE International Conference on Robotics and Automation (ICRA)*. IEEE, 2017, pp. 1944–1951.
- [34] R. V. Levine and A. Norenzayan, "The pace of life in 31 countries," *Journal of Cross-Cultural Psychology*, vol. 30, pp. 178–205, 1999.
- [35] T.-Y. Lin, M. Maire, S. Belongie, J. Hays, P. Perona, D. Ramanan, P. Dollár, and C. L. Zitnick, "Microsoft coco: Common objects in context," in *European conference on computer vision*. Springer, 2014, pp. 740–755.
- [36] J. Liang, Y.-L. Qiao, and D. Manocha, "Of-vo: Reliable navigation among pedestrians using commodity sensors," *arXiv preprint arXiv:2004.10976*, 2020.
- [37] Y. Wu, A. Kirillov, F. Massa, W.-Y. Lo, and R. Girshick, "Detectron2," <https://github.com/facebookresearch/detectron2>, 2019.
- [38] A. Dosovitskiy, P. Fischer, E. Ilg, P. Häusser, C. Hazirbaş, V. Golkov, P. v.d. Smagt, D. Cremers, and T. Brox, "FlowNet: Learning optical flow with convolutional networks," in *IEEE International Conference on Computer Vision (ICCV)*, 2015. [Online]. Available: <http://lmb.informatik.uni-freiburg.de/Publications/2015/DFIB15>
- [39] N. Mayer, E. Ilg, P. Häusser, P. Fischer, D. Cremers, A. Dosovitskiy, and T. Brox, "A large dataset to train convolutional networks for disparity, optical flow, and scene flow estimation," in *IEEE International Conference on Computer Vision and Pattern Recognition (CVPR)*, 2016, arXiv:1512.02134. [Online]. Available: <http://lmb.informatik.uni-freiburg.de/Publications/2016/MIFDB16>
- [40] J. S. Park and D. Manocha, "Efficient probabilistic collision detection for non-gaussian noise distributions," *IEEE Robotics and Automation Letters*, vol. 5, no. 2, pp. 1024–1031, 2020.